Thermochimica Acta, 150 (1989) 153–165
Elsevier Science Publishers B.V., Amsterdam – Printed in The Netherlands

THERMAL DECOMPOSITION AND CREATION OF REACTIVE SOLID SURFACES. VI. THERMAL GENESIS COURSE OF TITANIA CATALYST FROM A NOVEL AMMONIUM TITANYL OXALATE PRECURSOR

S.A.A. MANSOUR, G.A.M. HUSSEIN and M.I. ZAKI *

Chemistry Department, Faculty of Science, Minia University, El-Minia (Egypt)

(Received 31 January 1989)

ABSTRACT

The thermal decomposition course of ammonium titanyl oxalate monohydrate (ATO), $(NH_4)_2[TiO(C_2O_4)_2]\cdot H_2O$, was explored in view of its possible employment as a promising titania precursor in supported titania catalysts prepared by impregnation and subsequent calcination. The investigation implemented thermal analysis of ATO, and characterization of its gas and solid phase calcination products (at 100–800 °C) by means of infrared spectroscopy and X-ray diffractometry, to elucidate the pathways of the solid state reactions involved. The results revealed the occurrence of four endothermic weight loss processes (at 145–290 °C) leading to formation of amorphous (at > 200–300 °C), anatase-structured (at 350–700 °C) and rutile-structured (at ⩾ 800 °C) titania, via weight-invariant exothermic processes (maximized at 337, 408 and 773 °C). Non-isothermal kinetic parameters (k, A and ΔE) were calculated on the basis of the temperature shifts experienced at various heating rates (5, 10, 20 and 30 °C min^{-1}) by the thermal events encountered.

INTRODUCTION

Supported metal oxides are technologically an extremely important class of catalysts [1]. The primary aims in the preparation of these catalysts are to achieve maximum dispersion of the active phase on the support material and to stabilize this dispersion during heat treatments and under catalytic conditions [2]. There are two principal routes towards making these materials. The first, most frequently applied route involves impregnation of the support material, which is usually a high surface area oxide (YO), with a suitable precursor species of the active oxide (XO) from aqueous solution. The precursor is present in solution as either a cationic or anionic species. It is conceivable to assume that the dispersion of the active component in the final catalyst will be critically predetermined by the adsorption characteris-

* Author to whom correspondence should be addressed.

0040-6031/89/$03.50

tics of the ionic precursor species at the support/solution interface [3,4]. The second preparation route, which has stimulated further research [5–7], involves thermal treatments of physical mixtures of XO and YO. In this case, high dispersions can only be achieved if the active oxide is spread over the surface of the support oxide [8].

When dealing with the impregnation route, aqueous suspensions of the support oxide facilitate the occurrence of the following amphoteric dissociations of the surface hydroxyl groups

$$XOH_2^+ \rightleftharpoons XOH + H^+,\ K_1 \quad (1)$$

$$XOH \rightleftharpoons XO^- + H^+,\ K_2 \quad (2)$$

where K_1 and K_2 are the equilibrium constants of processes (1) and (2). There is a characteristic $pH = (pK_1 + pK_2)/2$ called the isoelectric point (IEP) at which a given immersed oxide surface has a zero net charge [9]. At a pH (furnished by the impregnating solution) above its IEP, the support surface is negatively charged, so that cations may be adsorbed [10]. In contrast, at a pH below its IEP, the support surface is positively charged leading to an adsorption of anions.

In view of the above-mentioned considerations, a compound such as that concerned in the present investigation, namely ammonium titanyl oxalate monohydrate, $(NH_4)_2[TiO(C_2O_4)_2] \cdot H_2O$, might be considered of importance to chemists who are engaged in the preparation of heterogenized analogues (TiO_2/Al_2O_3) of the Ziegler–Natta-type of polymerization catalysts [11], because Ti atoms are included in the anionic radical of the compound. When Al_2O_3 (IEP = 7.5–8.2 [9]) is immersed in an impregnating solution (pH 3–4) of this compound, the titanyl oxalate anions are preferentially strongly adsorbed.

In this part (VI) of the present comprehensive investigation [12(a–c)], the thermal genesis course of titania from ammonium titanyl oxalate has been closely examined by means of thermoanalytical, X-ray, and IR spectroscopic techniques. Non-isothermal kinetic parameters of the solid state processes involved have been calculated, on the basis of the temperature shifts experienced at various heating rates by the thermal events encountered.

EXPERIMENTAL

Materials

The ammonium titanyl oxalate [ATO = $(NH_4)_2[TiO(C_2O_4)_2] \cdot H_2O$] used was 99.98% pure, Aldrich (U.S.A.). Its calcination solid phase products were obtained at 100, 150, 200, 270, 350, 450, 600 and 800 °C for 2 h, in a still atmosphere of air. The calcination temperatures were chosen on the basis of

the thermal analysis results (see below). Prior to examination, the materials were kept dry over P_2O_5.

Thermal analysis

TG and DTA analyses of ATO were performed by heating at various rates ($\theta = 5$, 10, 20 and 30 °C min^{-1}) to 1000 °C, in a dynamic atmosphere of air (20 ml min^{-1}), using an automatically recording Shimadzu (Model 3OH) analyser (Japan). Typically, a 10–15 mg portion of the test sample was used for the TG, and highly sintered α-Al_2O_3 was the reference material for the DTA measurements.

Infrared spectroscopy

IR analysis of ATO and its calcination (gas and solid phase) products was carried out over the frequency range 4000–300 cm^{-1}, at a resolution of 5.3 cm^{-1}, by means of a Model 580B Perkin–Elmer spectrophotometer (U.K.). IR solid phase spectra were taken from thin (> 20 mg cm^{-2}), lightly loaded (< 1%) KBr-supported discs of the test sample. IR gas phase spectra were taken from the atmosphere surrounding a 0.5 g portion of ATO, being heated at 10 °C min^{-1} to various temperatures (100–450 °C for 10 min) in a specially designed IR cell [13] equipped with KBr windows. Prior to analysis, the cell was briefly evacuated (at 10^{-3} Torr for 5 m). In all cases the cell background spectrum was ratioed out using an on-line P–E Data Station (Model 3000).

X-ray diffractometry

XRD analysis of ATO and its solid phase calcination products was carried out by means of a Model JSX-60PA Jeol diffractometer (Japan), equipped with a source of Ni-filtered Cu $K\alpha$ radiation. For identification purposes, the diffraction patterns (I/I_0 versus d-spacing) obtained were matched with ASTM standards.

Kinetic analysis procedure of thermoanalytical data

From the resultant thermoanalytical curves, the temperatures (T_{max}) at which weight loss processes (TG) are maximized, or at the peak of the DTA curves corresponding to weight-invariant processes, were determined as a function of the heating rate (θ) applied.

The kinetic activation energy (ΔE, kJ mol^{-1}) was then calculated for each process from a plot of log θ against $1/T_{max}$, according to the relationship in the following equation [14]

$$\Delta E = -\frac{R}{b \, \mathrm{d} \log \theta / \mathrm{d}(1/T)} \tag{3}$$

where R is the gas constant (8.314 J mol^{-1} K^{-1}), θ is the heating rate (°C min^{-1}) and b is a constant (0.457).

Calculation of the frequency factor (A s^{-1}) of the weight loss processes involved was carried out, assuming first-order kinetics, using the following equation [15]

$$\log[-\log(1-C)/T^2] = \log AR/\theta\,\Delta E - \Delta E/2.303RT \quad (4)$$

where C is the fraction decomposed and T is the T_{max}. Having been determined, ΔE (from eqn. (3)) and A (from eqn. (4)) were used to calculate the reaction rate constant (k min^{-1}) adopting the Arrhenius equation

$$k = A\, e^{-\Delta E/RT} \quad (5)$$

RESULTS AND DISCUSSION

The results of the TG and DTA analyses of ATO are partly shown in Fig. 1 and further summarized in Table 1. They indicate that ATO decomposes via five endothermic weight loss processes (thermal events I–V), over the temperature range from 90 to 290 °C, leading to the formation of a solid material that suffers successive weight-invariant exothermic processes maximized at 337 °C (VI) and 408 °C (VII) prior to a slight weight loss process (VII) at 450–500 °C. The resultant product suffers a further weight-invariant exothermic process (IX), maximized at 773 °C (not shown in Fig. 1).

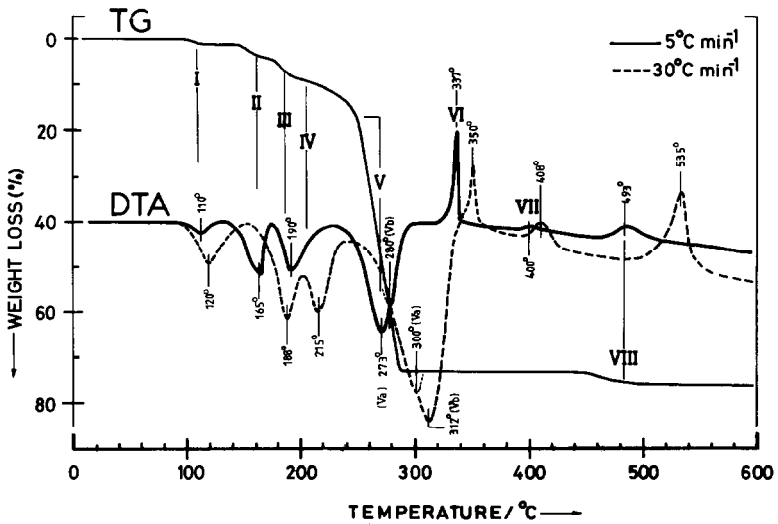

Fig. 1. TG and DTA curves recorded at the heating rates indicated for ammonium titanyl oxalate monohydrate, in a dynamic (20 ml min^{-1}) atmosphere of air. Characteristics of the events indicated (I–VIII) are summarized in Table 1.

TABLE 1

Characteristics of thermal events encountered throughout the thermal decomposition course of ATO (at 5 °C min^{-1})

Thermal [a] event	Temperature range (° C)	%Weight loss	$\Delta T/T$
I	90–120	1.0	endo
II	145–170	3.2	endo
III	170–190	4.3	endo
IV	190–240	6.5	endo
V [b]	240–290	57.5	endo
VI	337	–	exo
VII	408	–	exo
VIII	450–500	2.2	exo
IX	773	–	exo

[a] Weight loss processes manifested by events II–V are largely overlapping.

[b] Event V is shown by the corresponding DTA curve (Fig. 1) to be composite and to include two largely overlapping weight loss processes.

Characterization of thermal events encountered

I (at 90–120 °C)

Figure 1 and Table 1 show that the process involved in thermal event I causes a slight endothermic weight loss (~ 1.0%). The IR spectrum taken from the gas phase surrounding the ATO sample at 100 °C (Fig. 2) displays only a broad, weak absorption centred around 3400 cm^{-1}. This absorption

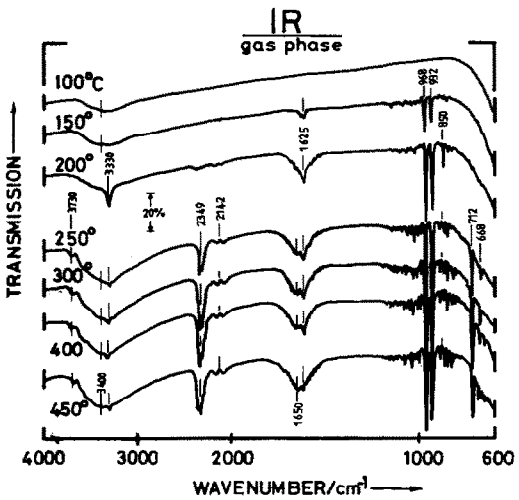

Fig. 2. IR spectra taken at a resolution of 5.3 cm^{-1} from the gas phase surrounding a 0.5 mg portion of ammonium titanyl oxalate monohydrate being heated (at 10 °C min^{-1}) at the temperatures indicated for 10 min.

indicates ν_{O-H} vibrations of hydrogen-bonded water molecules [16]. The absence of an absorption (normally observed at 1650–1600 cm^{-1} [16]) due to the δ_{O-H} vibrations, may be understood in view of the fact that it is more pressure sensitive than the ν_{O-H} absorption [17]. This result correlates well with the minor weight loss determined (~ 1.0%).

The IR spectrum and XR diffractogram of the solid-phase calcination product at 100 °C were very similar to those shown respectively in Figs. 3 and 4 for the untreated ATO. This may be because the water molecules released might have originated from the water of crystallization. Alternatively, it may suggest that thermal event I involves desorption of physisorbed water. The fact that the activation energy calculated (Table 3) amounts to a value (52.3 kJ mol^{-1}) well within the range characterizing physisorption processes ($\leqslant$ 60 kJ mol^{-1}), supports such a suggestion.

II (at 145–170 °C)

The gas phase released throughout thermal event II gives the 150 °C-spectrum exhibited in Fig. 2. The weak absorptions displayed therein (at 1625, 968 and 932 cm^{-1}) are diagnostic of NH_3 molecules [17]. An IR spectrum taken from the solid product at 150 °C consistently showed a weakening of the initial absorptions of NH_4^+, as originally exhibited in the spectrum of the untreated ATO (Fig. 3 and assigned in Table 2). Table 2 also summarizes the assignments of the other absorptions of ATO.

The weight loss determined (3.2%) by thermal event II (Fig. 1) is less than that expected (5.7%) for the release of ammonia contained in one mole of

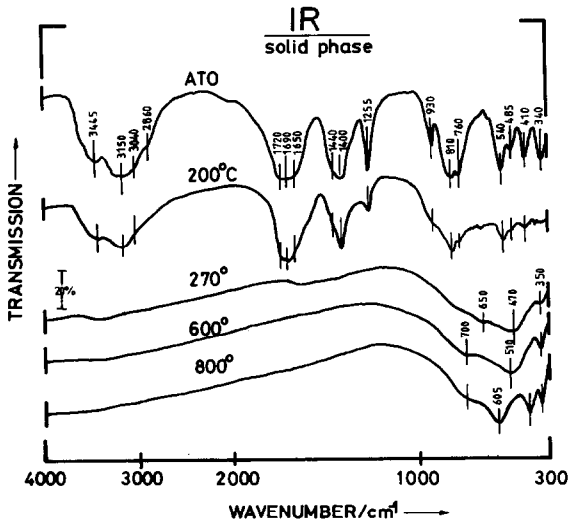

Fig. 3. IR spectra taken at a resolution of 5.3 cm^{-1} from KBr-supported samples of ammonium titanyl oxalate monohydrate (ATO) and its solid phase calcination products obtained at the temperatures indicated for 2 h.

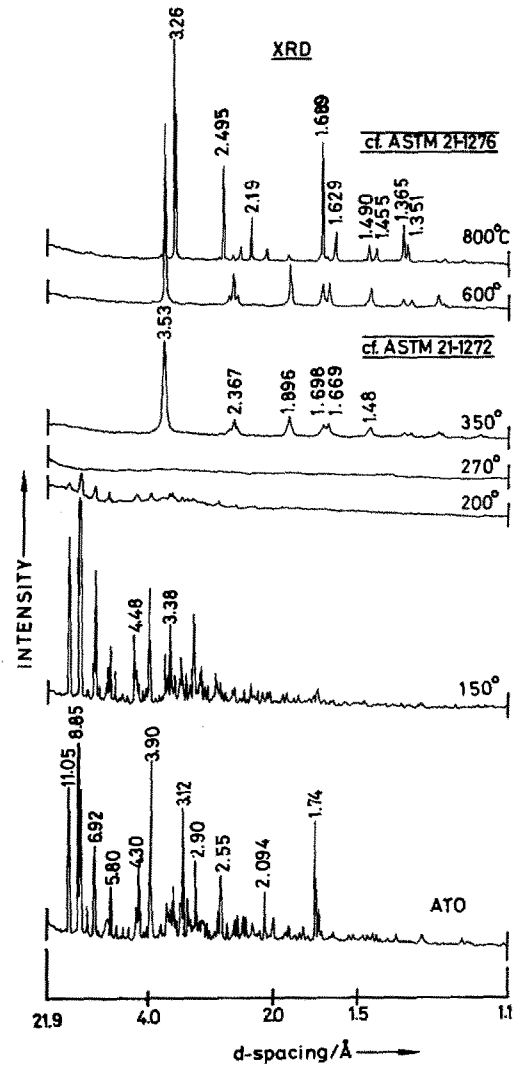

Fig. 4. X ray powder diffractograms (Cu $K\alpha$ radiation) for ammonium titanyl oxalate monohydrate (ATO) and its solid phase calcination products obtained at the temperatures indicated for 2 h.

NH_4^+ radicals. The XR diffractogram of the solid yielded at 150 °C (Fig. 4) only retains the strongest lines of ATO (observed at $\geqslant 2.9$ Å) and, in addition, displays two moderate, unidentified lines at 4.48 and 3.38 Å. These results may suggest that the decomposition of one mole of NH_4^+ radicals leads to a modification of the infrastructure of the original ATO lattice, without, however, causing a significant loss of crystal coherency.

III (at 170–190 °C)

The IR gas phase spectrum at 200 °C (Fig. 2), i.e. encompassing the weight loss step experienced in thermal event III (Fig. 1), shows that the

TABLE 2

Assignments for IR absorptions observed in the spectrum (Fig. 3) taken from ATO $\{(NH_4)_2[TiO(C_2O_4)_2]\cdot H_2O\}$

Frequency (cm^{-1})	Assignment	Ref.
3445	ν_{O-H} (H-bonded)	16
3150	NH_4^+ (ν_3)	24
3040	NH_4^+ (ν_1)	24
2860	NH_4^+	24
1720	$\nu_{a,C=O}$ (ν_7)	25
1690	$\nu_{a,C=O}$ (ν_1)	25
1650	$\nu_{a,C=O}$ (ν_1) + δ_{H_2O}	25, 16
1440	NH_4^+ (ν_4)	24
1400	$\nu_{S,C=O}$ (ν_2) + ν_{C-O}	25
1255	$\nu_{S,C=O}$ (ν_8) + $\delta_{O-C=O}$	25
930	$\nu_{Ti=O}$	19
810	$\nu_{O-C=O}$ (ν_9)	25
760 [a]	ν_{Ti-O}	25
540	ν_{Ti-O} (ν_4) + ν_{C-C}	25
485	ring deformation (ν_{10}) + $\delta_{O-C=O}$	25
410	ν_{Ti-O} (ν_{11}) + ring deformation	25
340	$\delta_{O-C=O}$ + ν_{C-C}	25

[a] Torsional oscillations of water of crystallization contribute to absorptions at $\leqslant 700$ cm^{-1}, ref. 26.

NH_3 absorptions at 968 and 932 cm^{-1} have almost doubled their intensities observed at 150 °C, and also shows its other pressure-sensitive absorptions at 3330 and 850 cm^{-1} [17]. In fact, the intensities exhibited by the NH_3 absorptions at 200 °C have suffered an insignificant increase ($\sim 1.5\%$) on heating to 450 °C (Fig. 2). This observation, together with the fact that the gas phase spectra were recorded under almost identical spectroscopic conditions, may support the suggestion that thermal event III involves the release of the ammonia contained in the second mole of NH_4^+ radicals. Consistent with this, the total weight loss (7.5%) effected by events II and III is twice that caused by event I alone (3.2%). It is worth mentioning, however, that the total weight loss observed is still less then expected (11.6%) for the release of the ammonia contained in two moles of NH_4^+ radical. This may imply that event III does not actually terminate at 190 °C, as given in Table 1, but goes on beyond this temperature to be overlapped by the succeeding event IV.

The IR spectrum taken from the solid material produced at 200 °C (Fig. 3) shows an almost complete absence of NH_4^+ absorptions (cf. Table 2). The corresponding XRD (Fig. 4) indicates that the product has lost most of the original crystallinity of ATO. As the IR spectrum still displays most of the diagnostic absorptions of the oxalate ligands and the titanyl group, as well

TABLE 3

Non-isothermal kinetic parameters [a] of the thermal events encountered throughout the decomposition course of ATO

Thermal event	k (min^{-1})	log A	ΔE (kJ mol^{-1})
I	–	–	52.3
II	0.752	14.70	75.4
III	1.188	22.36	140.0
IV	0.438	9.18	65.8
V [b]	1.302	23.55	163.3
VI	–	–	196.0
VII	–	–	490.5
VIII	0.833	17.63	158.1

[a] Kinetic parameters of thermal events II–V and VIII were calculated from TG data, whereas for the other events (I, VI and VII) the DTA data were used.

[b] On the basis of the DTA data (Fig. 1), thermal event V is a composite feature involving two overlapping processes Va (273–300 °C) and Vb (280–312 °C), for which the calculated ΔE values are respectively 140.2 and 98.1 kJ mol^{-1}.

as the absorptions of the water of crystallization, it can be seen that the NH_4^+ radicals contribute actively to the linkages responsible for the ATO crystal coherency. Table 3 allocates an activation energy value (140.0 kJ mol^{-1}) for thermal event III that is twice the value (75.4 kJ mol^{-1}) calculated for thermal event II. This result may suggest that either the two moles of NH_4^+ radicals are initially of disparate thermal stabilities, or that as the first mole decomposes (at 145–170 °C) the second becomes simultaneously more strongly bound.

IV (at 190–240 °C)

The TG curve (Fig. 1) shows that thermal event IV occurs slowly and is largely overlapped by the succeeding event V. This observation can be supported by the corresponding rate constant value (Table 3). The IR gas phase spectrum at 250 °C (Fig. 2) exhibits a considerable reinforcement in the ν_{O-H} absorption (around 3400 cm^{-1}) and the emergence of the pressure-sensitive δ_{O-H} absorption at 1650 cm^{-1}. It shows additional absorptions due to CO_2 (at 3730, 2349, 712 and 668 cm^{-1} [17]) and CO (weak bands centred around 2142 cm^{-1} [17]).

The solid material produced at 250 °C gave an IR spectrum documenting the disappearance of absorptions due to stretching (at 3500–3200 cm^{-1}), bending (at 1650 cm^{-1}) and torsional oscillations (at < 700 cm^{-1}) of crystallization water. It also revealed an insignificant decrease in the absorption intensities shown in the 200 °C-spectrum for the oxalate ligands. These results may presume that thermal event IV predominantly involves the elimination of the water of crystallization; the coexistence of CO_2 and CO

molecules in the gas phase derives from the overlapping thermal event V. In fact, the corresponding activation energy (65.8 kJ mol^{-1}) is of the same order of magnitude of energy values reported elsewhere [18] for removal of crystallization water from analogous compounds.

The XRD analysis performed on the material produced at 250 °C indicated an entirely amorphous nature; the pattern obtained was very similar to that shown in Fig. 4 for the 270 °C-product. This suggests a complete collapse of the initial crystalline structure of ATO. As a result, it may be presumed that the H_2O molecules cooperate with the NH_4^+ radicals in providing the primary linkages (probably hydrogen bonds) responsible for the ATO crystal coherency.

V (240–290 °C)

The TG curve given in Fig. 1 shows that thermal event V involves the most prominent weight loss (57.5%) encountered throughout the decomposition course of ATO. On the other hand, the corresponding DTA curve (Fig. 1) reveals its composite nature by exhibiting a strong endothermic effect of two maxima at 273 and 280 °C.

The observed total weight loss (71.5%) completed at 290 °C is very close to that (72.8%) expected for the conversion of ATO to TiO_2. The IR spectrum taken from the solid yielded at 270 °C (Fig. 3) indicates the disappearance of the band structure characterizing the titanyl oxalate, and shows instead a strong and broad, composite absorption of three components centred around 650, 470 and 350 cm^{-1}. The XR diffractogram (Fig. 4) reveals an amorphous nature for the material.

The IR spectrum taken from the gas phase at 300 °C (Fig. 2) indicates that the characteristic absorptions of CO_2 molecules have notably increased in intensity, whereas those diagnostic of CO have suffered an insignificant intensity increase. This may suggest that thermal event V involves two strongly overlapping processes. The earlier process, marked by the endothermic maximum at 273 °C (Fig. 1), may involve the release of the CO molecules, whereas the succeeding process (signified by the endothermic maximum at 280 °C) may include the elimination of the CO_2 molecules. The corresponding activation energy values (cf. footnote of Table 3) reveal that the release of CO_2 (98.1 kJ mol^{-1}) is energetically easier than the elemination of CO (140.2 kJ mol^{-1}), a result that might explain the strong overlapping of the corresponding weight loss steps (Fig. 1).

To summarize, thermal event V involves the decomposition of the oxalate ligands, and a consequent release of CO molecules leading to the conversion of the oxalate to carbonate, which immediately decomposes, releasing CO_2 molecules, eventually giving TiO_2. Recent research work, reported elsewhere [19], has shown that nearly all of the oxotitanium compounds, including the sulphate and oxalate, actually contain –Ti–O–Ti–O– chains rather than TiO^{2+} units, thus suggesting their existence in di- or trimeric form. There-

fore, the amorphous nature observed for the solid product at 270 °C would be a result of a further, simultaneous polymerization and lattice reorganization on the way to TiO_2 formation.

VI (at 337 °C)

Thermal event VI indicates an exothermic, weight-invariant process. The solid material produced at 350 °C gave rise to IR absorption characteristics very similar to those shown in Fig. 3 for the 600 °C-product. These are slight high-frequency shifts of the component absorptions at 650 (to 700 cm^{-1}) and at 470 (to 510 cm^{-1}) along with a slight increase in the 350 cm^{-1}-absorption intensity. These modifications indicate [20] the build-up of an anatase-like structure for titania. Consistent with this, the XR diffractogram obtained for the 350 °C-product (Fig. 4) matches well with the pattern (ASTM 21-1276) of a standard anatase-structured TiO_2. Therefore, the exotherm at 337 °C must have accompanied the crystallization process involved.

VII (at 408 °C)

Thermal event VII also indicates an exothermic, weight-invariant process. It shows the highest activation energy (490.5 kJ mol^{-1}), of all the events encountered. The solid product at 450 °C gave rise to an XRD pattern similar to that shown in Fig. 4 for the 600 °C-product, and indicates a considerable advance towards crystallization of TiO_2 into the anatase structure. In turn, this may suggest that the ordering mechanism involved occurs in two energetically distinguished steps.

VIII (at 450–500 °C)

The thermoanalytical results given in Fig. 1 show that thermal event VIII involves a slight weight loss process (2.2%). The IR gas phase spectrum at 450 °C (Fig. 2) differs from the 400 °C-spectrum in showing a slight increase in the absorptions (at 3400 and 1650 cm^{-1}) due to water molecules. This suggests that the volatile component released throughout event VIII is water.

Because the weight loss determined (2.2%) by this event is far less than expected (18%) for the elimination of one mole of water molecules, the process involved may be seen as a condensation-type reaction occurring at the expense of surface OH groups [21]. However, the exothermic nature revealed by the corresponding DTA curve (Fig. 1) for the reaction may suggest a topochemical conduct including atmospheric oxygen [22].

IX (at 773 °C)

The process involved in thermal event IX is an exothermic, weight-invariant one. The IR spectrum taken from the solid produced after calcination at 800 °C differs from that exhibited by the 600 °C-product in displaying strong component absorptions at 605 and 420 cm^{-1}. Both of these

features, together with the absorptions at 700 and 350 cm^{-1}, characterize a rutile-structured TiO_2 [20]. Strong support for this assignment is provided by the corresponding X ray diffractogram, which displays a pattern that matches well with the pattern (ASTM 21-1276) of a standard rutile-structured TiO_2. The exotherm at 773° C can therefore be taken to mark the anatase → rutile transition of TiO_2.

CONCLUSIONS

The following conclusions can be drawn from the above described and discussed results:

(1) The course of the thermal genesis of TiO_2 from ammonium titanyl oxalate monohydrate may include the following pathways

$$(NH_4)_2[TiO(C_2O_4)_2] \cdot H_2O \xrightarrow{II} (NH_4)H[TiO(C_2O_4)_2] \cdot H_2O$$

$$\xrightarrow{III} H_2[TiO(C_2O_4)_2] \cdot H_2O \xrightarrow{IV} H_2[TiO(C_2O_4)_2]$$

$$\xrightarrow{V} \underset{(\text{where } x < 1)}{\text{am. } TiO_2 \cdot xH_2O} \xrightarrow{\text{VI and VII}} \underset{(\text{anatase})}{\text{cry. } TiO_2 \cdot xH_2O} \xrightarrow{VIII} \underset{(\text{anatase})}{\text{cry. } TiO_2}$$

$$\xrightarrow{IX} \underset{(\text{rutile})}{\text{cry. } TiO_2}$$

where the Roman numeral denotes the relevant thermal event (see Table 1).

(2) The complete decomposition of ATO at a temperature as low as 290° C with the formation of amorphous titania may favour its employment as a precursor to well-dispersed titania in supported catalyst systems. As a matter of fact, decompositon of catalyst precursors at higher temperatures may hamper their application, as an influencing sintering of the support material may simultaneously occur [23].

REFERENCES

1 D.L. Trimm, Design of Industrial Catalysts, Chemical Engineering Monographs, Vol. 11, Elsevier, Amsterdam, 1980.

2 B. Delmon, P. Grange, P.A. Jacobs and G. Poncelet (Eds.), Preparation of Catalysts II, Elsevier, Amsterdam, 1979.

3 J. Leyrer, B. Vielhaber, M.I. Zaki, Zhuang Shuxian, J. Weitkamp and H. Knözinger, Mater. Chem. Phys., 13 (1985) 301.

4 H.M. Ismail, C.R. Theocharis and M.I. Zaki, J. Chem. Soc., Faraday Trans. I, 83 (1987) 2835.

5 Y. Xie, L. Gui, Y. Liu, Y. Zhang, B. Zhao, N. Yang, O. Guo, L. Duan, H. Huang, X. Cai and Y. Tang, in M. Che and G.C. Bond (Eds.), Adsorption and Catalysis on Oxide Surfaces, Elsevier, Amsterdam, 1985, p. 139.

6 J. Haber, T. Machej and T. Czeppe, Surf. Sci., 151 (1985) 301.
7 R. Margraf, J. Leyrer, E. Taglauer and H. Knözinger, React. Kinet. Catal. Lett., 35 (1987) 261.
8 J. Leyrer, M.I. Zaki and H. Knözinger, J. Phys. Chem., 90 (1986) 4775.
9 G.A. Parks, Chem. Rev., 65 (1965) 177.
10 J.P. Brunelle, Pure Appl. Chem., 50 (1978) 1211.
11 K. Ziegler, E. Holzkamp, H. Breil and H. Martin, Angew. Chem., 67 (1955) 541; G. Natta, J. Polymer Sci., 16 (1955) 145.
12 (a) M.I. Zaki and M. Abdel-Khalik, Thermochim. Acta, 78 (1984) 29; (b) M.I. Zaki and M. Abdel-Khalik, Colloids and Surfaces, 13 (1985) 323; (c) M.I. Zaki and R.B. Fahim, J. Therm. Anal., 31 (1986) 825; (d) M.I. Zaki and N.E. Fouad, Thermochim. Acta, 95 (1985) 73; (e) S.A.A. Mansour, M.A. Mohamed and M.I. Zaki, Thermochim. Acta, 129 (1988) 187.
13 J.B. Peri, and R.B. Hannan, J. Phys. Chem., 64 (1960) 1526.
14 J.H. Flynn and A. Wall, Polym. Lett. B, 4 (1966) 323; J.H. Flynn, J. Therm. Anal., 27 (1983) 45.
15 A.W. Coats and J.P. Redfern, Nature (London), 201 (1964) 68.
16 J.A. Gadsden, Infrared Spectra of Minerals and Related Inorganic Compounds, Butterworths, London, 1975, pp. 15–16.
17 R.H. Pierson, A.N. Fletcher and E. St. Clair Gabtz, Anal. Chem., 28 (1956) 1218.
18 W.E. Brown, D. Dollimore and A.K. Galwey, in C.H. Bamford and C.F.H. Tipper (Eds.), Chemical Kinetics Vol. 22: Reactions in the Solid State, Elsevier, Amsterdam, 1980, pp. 130–135.
19 R.J.H. Clark, in J.C. Bailar, Jr., H.J. Emeléus, N. Nyholmand A.F. Trotman-Dickenson (Eds.), Comprehensive Inorganic Chemistry, Vol. 3, Pergamon Press, Oxford, 1975, pp. 377–379.
20 N.T. McDevitt and W.L. Baun, Spectrochim. Acta, 20 (1964) 799.
21 G.A.M. Hussein, N. Sheppard, M.I. Zaki and R.B. Fahim, J. Chem. Soc. Faraday Trans. I, 1989, in press.
22 Ref. 18, pp. 144–151.
23 Ref. 1, pp. 91–103.
24 K. Nakamoto, Infrared and Raman Spectra of Inorganic and Coordination Compounds, 3rd edn., Wiley New York, 1978, pp. 132–135.
25 Ref. 24, pp. 233–238.
26 F.A. Miller, G.L. Carlson, F.F. Bentley and W.H. Jones, Spectrochim. Acta, 16 (1960) 135.